ACS OMEGA

http://pubs.acs.org/journal/acsodf

Article

Bispecific Aptamer Sensor toward T-Cell Leukemia Detection in the Tumor Microenvironment

Natalie Boykoff,[⊥] Lina Freage,[⊥] Jared Lenn, and Prabodhika Mallikaratchy*

Cite This: *ACS Omega* 2021, 6, 32563−32570

Read Online

ACCESS | Metrics & More | Article Recommendations | Supporting Information

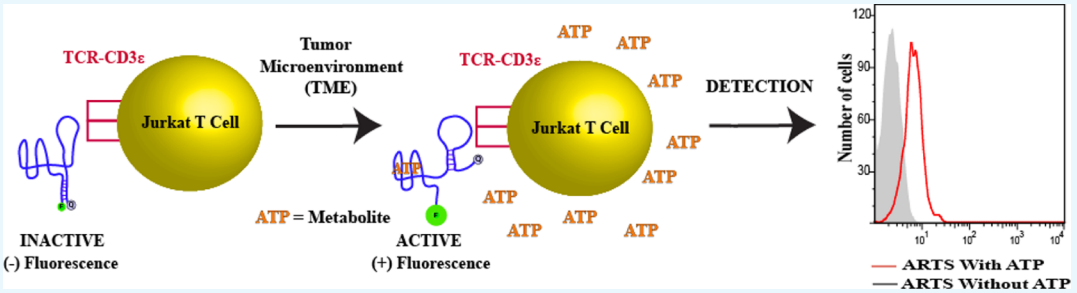

ABSTRACT: The current detection methods of malignant cells are mainly based on the high expression levels of certain surface proteins on these cells. However, many of the same surface marker proteins are also expressed in normal cells. Growing evidence suggests that the molecular signatures of the tumor microenvironment (TME) are related to the biological state of a diseased cell. Exploiting the unique molecular signature of the TME, we have designed a molecular sensing agent consisting of a molecular switch that can sense the elevated concentration of a small molecule in the TME and promote precise recognition of a malignant cell. We accomplished this by designing and developing a bispecific aptamer that takes advantage of a high concentration of adenosine 5′-triphosphate in the TME. Thus, we report a prototype of a bispecific aptamer molecule, which serves as a dual detection platform and recognizes tumor cells only when a given metabolite concentration is elevated in the TME. This system overcomes hurdles in detecting tumor cells solely based on the elevated expression of cell surface markers, providing a universal platform for tumor targeting and sensing.

INTRODUCTION

Unlike normal cells, malignant cells sustain their rapid anabolic and energy production rates by requiring extraordinary high levels of nutrients.[1−3] This altered metabolic state of tumor cells and their interaction with the surrounding tissues form a unique microenvironment termed tumor microenvironment (TME).[4] The biochemical composition of the TME is based on the survival of tumor cells and their need to mitigate the competition for nutrients by surrounding cells.[3,5]

Additionally, the unique chemical signatures of the TME could characterize the tumor cell's own metabolic needs and waste products as a reflection of their biological state.[1−7] The TME also assists tumor cells in escaping immune surveillance, orchestrating a remarkable ability to adapt and survive.[6,7] Accordingly, the detection and modulation of the TME's biochemical composition could be an exciting avenue for tumor-targeting owing to its prominent role in the initiation and survival of tumors.[8−10] The TME is characterized by abnormal fluctuations, including hypoxia (low oxygen levels), low extracellular pH (ranging from 6.5 to 6.8) resulting from the upregulation of glycolysis, and the atypical expression of tumor-related enzymes.[11,12] Recently, the adenosine 5′-triphosphate (ATP) concentration was found to be around 100 μM, which is about 1000−10 000 times higher within the TME than that of the typical cellular environment, indicating that the concentration of ATP can be utilized as a secondary biomarker to detect tumor cells.[7,13−15]

The cell−surface molecular signatures of diseased cells have been the focal point for the design and engineering of diagnostic and therapeutic targeting molecules against tumor cells.[16−18] Indeed, a cell's pathological state is highly correlated to elevated expression levels of particular molecular signatures on the cell surface. However, many of these same surface marker proteins are also expressed in normal cells leading to higher background signals.[19] Consequently, significant research efforts are now centered on detecting altered cellular pathological states using molecules secreted by malignant cells, such as exosomes, microRNAs, proteins, and other metabolic molecules unique to the tumor cell's metabolic

Received: August 2, 2021
Accepted: October 6, 2021
Published: November 19, 2021

states.[19−22] The primary biomarker protein-related tumorigenesis and the unique metabolic state of the TME can be utilized as a secondary marker to enhance the specificity of detection. Thus, we herein sought to explore the utility of the TME's unique chemical signature as an avenue to detect tumor cells and their elevated protein expression specifically. We accomplished this by designing a bispecific aptamer with one arm toward a highly expressed tumor-related metabolite ATP and the other arm toward a cell surface marker expressed on a human T-cell lymphoma.[23,24] Thus, the functional bispecific aptamer molecule, described here, effectively combines two molecular signatures related to a disease state, namely, altered ATP concentration in TME and an elevated expression of the cell surface marker TCR-CD3ε in T-cells.

This prototype bispecific sensor model is termed ATP-regulated T cell sensor (ARTS), which contains an ATP aptamer and an aptamer against TCR-CD3ε expressed on T-cells. The ARTS molecule is designed to sense the elevated concentration of ATP in the TME, which then subsequently undergoes a conformational switch, allowing the tumor-specific arm of the bispecific aptamer to bind to the CD3 + T cell leukemia by targeting through the TCR-CD3ε receptor (Scheme 1). By combining two aptamers, we demonstrate that a bispecific sensor molecule with dual specificity can serve as a superior detection platform that can recognize diseased cell states with higher precision.

RESULTS AND DISCUSSION

The bispecific aptamer consists of a two stacked G-quartets ATP aptamer and an anti-CD3ε aptamer linked with two tandem units of hexaethylene glycol spacer (6 repeats, 24 carbon spacers). Each terminus is labeled with a fluorophore and a quencher. We designed the structure-switching bispecific aptamer by modifying the anti-CD3ε aptamer with a complementary strand that can hybridize with the ATP aptamer. We accomplished this design based on the previously reported structure and function study of the ATP aptamer.[23] Huizenga and Szostak predicted that the DNA aptamer against ATP forms two stacked G-quartets with a mutable stem region.[23] Therefore, we have modified the anti-CD3ε aptamer's stem complementary to the $C_{(1)}A_{(2)}C_{(3)}C_{(4)}T_{(5)}G_{(6)}G_{(7)}G_{(8)}$ of the ATP aptamer. This eight base-pair duplex structure effectively disrupts the predicted two-stacked G-quartets of the ATP aptamer and the stem-loop structure of the anti-CD3ε aptamer resulting in inactive conformations. However, the presence of the ATP drives the formation of the two stacked G-quartet structures, while releasing the anti-CD3ε aptamer's stem-loop structure enabling the T-cell lymphoma detection.

The ARTS design consists of two states. State A consists of an inactive anti-CD3ε aptamer and an ATP aptamer arranged such that the functional folds of both aptamers are disrupted to form a stable duplex (Scheme 1I), bringing the fluorophore and the quencher in close proximity, resulting in a quenched fluorescence.

In state B, this duplex between the two aptamers can be destabilized through a conformational switch induced by ATP binding to the ATP aptamer, simultaneously generating a fluorescence signal while, at the same time, releasing the primary aptamer against TCR-CD3ε, enabling the detection of T-cell lymphoma. We designed two control molecules for this bispecific aptamer. The first control molecule randomizes the ATP aptamer. Termed ARTS-R1, this controller prevents the

Scheme 1. Design of the Bispecific Aptamer Facilitating a Conformational Change from State A to State B; (I) ARTS, (II) Control-1 with Randomized ATP Sequence (ARTS-R1), and (III) Control-2 with Randomized Anti-CD3ε Aptamer (ARTS-R2); All Three Molecules Possess 6-FAM and IBFQ on Their 5′ and 3′ Ends, Respectively; State A is Stable in the Absence of the ATP; That is, in This State, the Duplex Structure is Stable, and the Two Reporting Molecules, 6-FAM and Iowa Black, Are in Close Proximity, Enabling Fluorescence Energy Transfer; State B Shows the Open Conformation, Which Is Triggered by the Presence of ATP Molecules, Allowing the Anti-CD3ε Aptamer to Detect CD3ε on Jurkat.E6 Cells

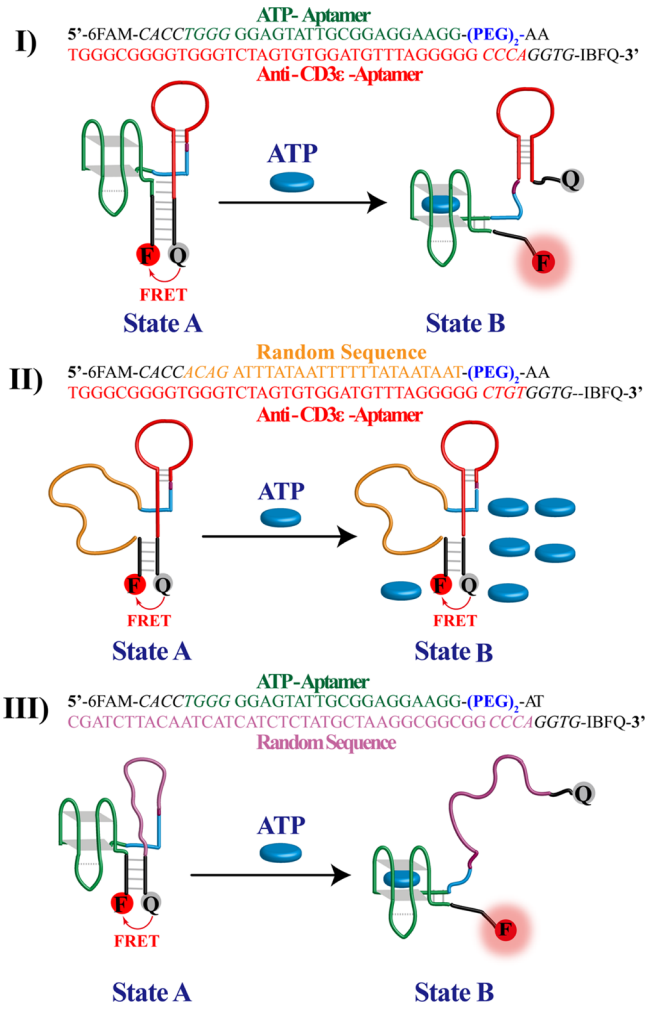

conformational switch of the ATP aptamer in the presence of ATP (Scheme 1II). The second controller, termed ARTS-R2, randomizes an anti-CD3ε aptamer (Scheme 1III). Under the control of ARTS-R2, the binding of ATP to the ATP aptamer leads to a conformational switch promoting state B, as described above. However, although the fluorescence is increased, the anti-CD3ε detection on the T-cell lymphoma is not possible.

We first evaluated the thermal stability of ARTS by measuring the fluorescence intensity of the FAM fluorophore as a function of temperature. Below the melting point, ARTS forms a stable duplex structure (state A), leading to no detectable fluorescence signals in the system (Figure 1A−C). However, while the ARTS duplex structure is stable at

https://doi.org/10.1021/acsomega.1c04125
ACS Omega 2021, 6, 32563−32570

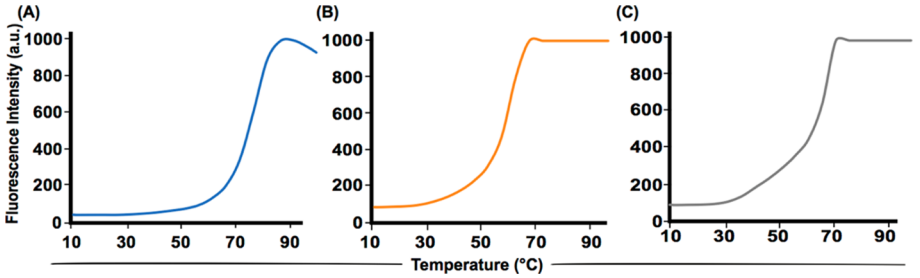

Figure 1. Thermal stability analysis as measured by fluorescence intensity as a function of temperature. (A) ARTS, (B) ARTS-R1, and (C) ARTS-R2 at different temperatures.

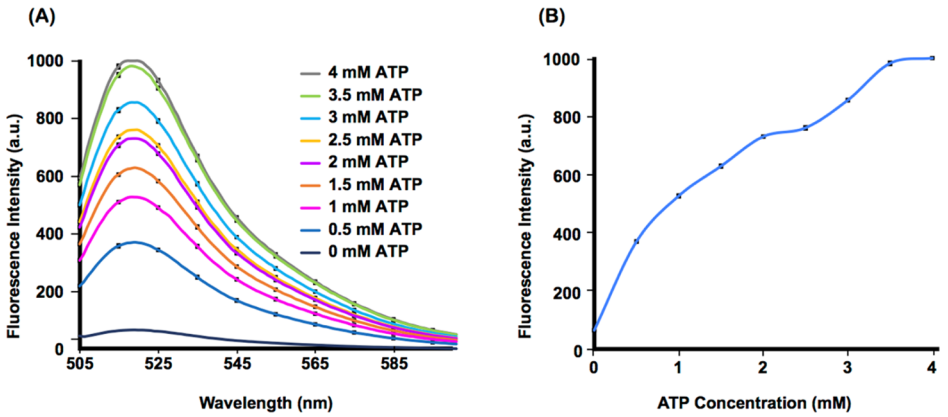

Figure 2. Change of the fluorescence intensity of ARTS as a function of ATP concentration. (A) Fluorescence spectrum of ARTS in the absence of ATP and with 0.5, 1, 1.5, 2, 2.5, 3, 3.5, and 4 mM of ATP; (B) titration plot of ATP incubated with ARTS over the range of 0−4 mM ATP. The ARTS was prepared for the assay by heating at 95 °C for 5 min and then cooling down to 25 °C for 30 min. Nine samples of 250 nM ARTS and different concentrations of ATP were prepared in a final volume of 500 μL of tris-HCl buffer (10 mM, pH = 8.4) and 6 mM $MgCl_2$, followed by placing in a Cary Eclipse fluorescence spectrophotometer at 25 °C. Fluorescence spectra were produced with an error = ±~2.

temperatures well below its melting temperature at 75.2 °C, the gradual increase of temperature beyond the melting point leads to a disruption of each aptamer's duplex structure, generating a single-stranded DNA (Figure 1A−C). These results show the high thermostability of ARTS in physiological temperature.

Next, the sensitivity of ARTS was analyzed as a function of the concentration of ATP (Figure 2A). The experiments were conducted using a fixed concentration of ARTS at 250 nM in tris-HCl buffer (10 mM, pH = 8.4) and 6 mM $MgCl_2$. The initial baseline fluorescence signal was indicative of state A (absence of ATP), which was first recorded. Then ATP was added in a stepwise manner at 0.5, 1, 1.5, 2, 2.5, 3, 3.5, and 4 mM concentrations. The fluorescence signal increased immediately after the addition of 0.5 mM ATP, indicating that the addition of ATP leads to a conformational switch (Figure 2A). The subsequent addition of ATP further increased the fluorescence signal saturating at a concentration of 3.5 mM ATP, presenting a linear relationship between the fluorescence enhancement and ATP concentration that resulted from the conformational switch (Figure 2B). The controls were also tested with different concentrations of ATP. As anticipated, the fluorescence intensity of ARTS-R2 increased as a function of ATP concentration in a manner similar to that of ARTS. In contrast, no significant change in the fluorescence signal was observed for ARTS-R1 in the absence or presence of ATP, demonstrating the sensitivity and the specificity of the conformational switch in response to the presence of ATP (Figures S1 and S2).

We next examined the sequence specificity of the conformational change induced by ATP using 250 nM of ARTS, ARTS-R1, or ARTS-R2 in tris-HCl buffer (10 mM, pH = 8.4) and 6 mM $MgCl_2$. After recording the background fluorescence of ARTS in the absence of ATP, 2 mM ATP were added. As expected, ARTS-R1 showed no change in fluorescence in the presence of ATP compared to ARTS (Figure 3A,B). In contrast, ARTS-R2 with a randomized anti-CD3ε aptamer did undergo a conformation change in the presence of ATP, leading to an enhanced fluorescence signal (Figure 3C), confirming that the CD3ε-specific DNA sequence does not affect the conformational change of the ATP aptamer. We observed that the fluorescence enhancement for ATRS-R2 is lower than that of ARTS (Figure 3D). Even though the ATP releases the control anti-CD3ε sequence releasing the fluorophore, the randomization of the anti-CD3ε may have led to the formation of undesired intramolecular interactions leading to secondary folds, which could bring the fluorophore and the quencher to close physical proximity leading to partial fluorescence quenching. Such observations have been previously observed in the design of molecular beacons.[25]

To investigate the nucleotide specificity of ARTS, we tested the conformational change of the ARTS constructs in the presence of different nucleotides. The change of the fluorescence signal was measured in the presence of ATP (blue line in Figure 4A−C), guanosine-5′-triphosphate (GTP) (yellow line in Figure 4A), cytidine-5′-triphosphate (CTP) (yellow line in Figure 4B), and uridine-5′-triphosphate (UTP) (yellow line in Figure 4C). We did not observe a significant increase in the fluorescence signal with control nucleotides

https://doi.org/10.1021/acsomega.1c04125
ACS Omega 2021, 6, 32563−32570

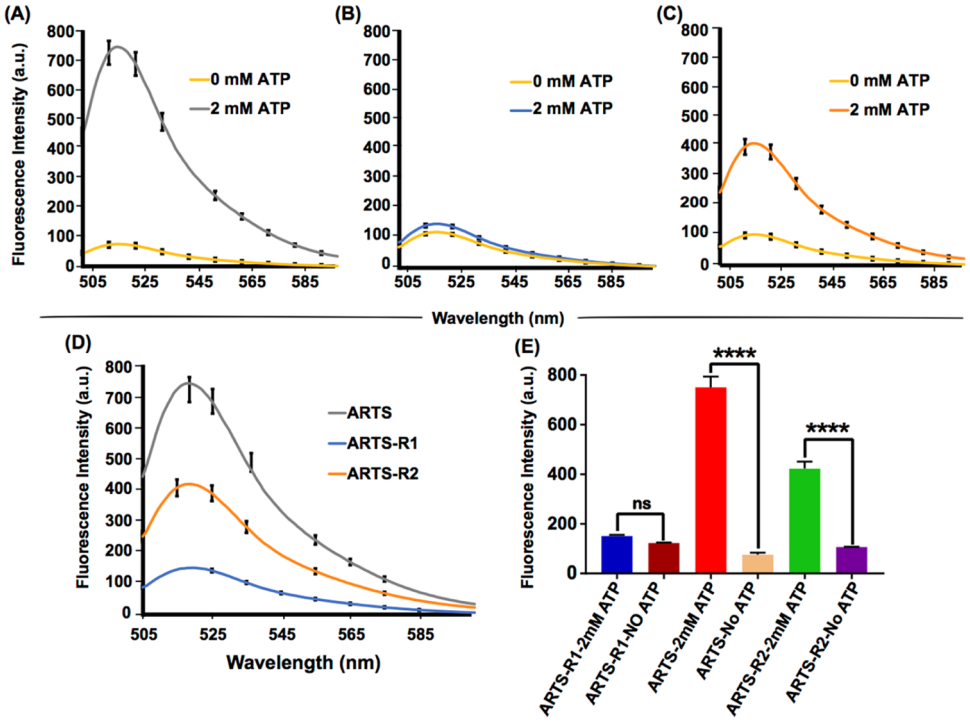

Figure 3. Fluorescence spectra of the FAM fluorophore of ARTS, ARTS-R1, and ARTS-R2 in the absence and presence of ATP. The fluorescence spectrum of (A) ARTS, (B) ARTS-R1, and (C) ARTS-R2 in the absence and presence of 2 mM ATP. (D) Direct comparison of spectra for the three aptamer constructs in the presence of 2 mM ATP. (E) Bar graph of fluorescence intensity of the aptamers in the presence and absence of 2 mM ATP, reflecting the outcome of three independent specific binding experiments with and without the addition of ATP, using one-way analysis of variance (ANOVA) with the Student's *t*-test performed on GraphPad Prism ns: $p \leq 0.0001$, ****: $p \leq 0.0001$.

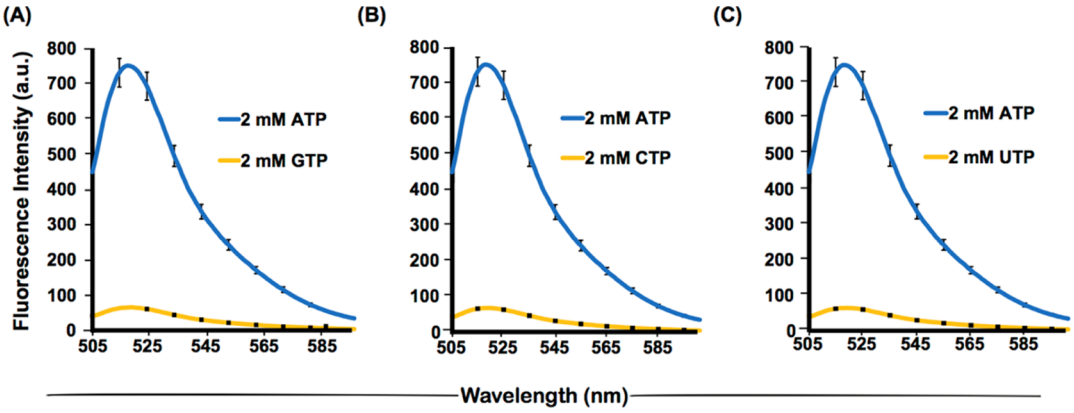

Figure 4. Analysis of the specificity of the ATP aptamer in ARTS. (A) Specificity of ATP aptamer in ARTS with 2 mM ATP and 2 mM GTP, as measured by fluorescence intensity. (B) Specificity of the ATP aptamer in ARTS with 2 mM ATP and 2 mM CTP. (C) Specificity of the ATP aptamer in ARTS with 2 mM ATP and 2 mM UTP. ARTS was prepared by heating at 95 °C for 5 min and then cooling down to 25 °C over a period of 30 min. Six samples of 250 nM ARTS were prepared in tris-HCl buffer (10 mM, pH = 8.4) and 6 mM $MgCl_2$. To each sample was added ATP, GTP, CTP, or UTP at a final concentration of 2 mM.

suggesting the specificity of ARTS toward ATP. The control molecules ARTS-R1 and ARTS-R2 were also tested and showed no significant change in fluorescence intensity after the addition of GTP, CTP, or UTP (Figures S3 and S4).

SPECIFIC BINDING TO JURKAT E6.1 CELLS

We next evaluated the specific recognition of T-cell leukemia known to express high levels of TCR-CD3ε. ARTS is a bifunctional sensor, first detecting the presence of an altered biochemical composition in the TME, followed by the presence of tumor cells. To test anti-CD3ε binding, 100 nM of ARTS, or its controls, were combined in a solution with 500 μM ATP, followed by incubation for 1 h with 1×10^5 Jurkat E6.1 cells. Although ARTS specifically recognized Jurkat.E6 cells in the presence of ATP, no specific cell binding was observed for ARTS-R1 and ARTS-R2, suggesting the ability of ARTS to detect Jurkat.E6 cells specifically (Figure 5A–E). The affinity of the anti-TCR-CD3 aptamer segment in ARTS toward TCR-CD3ε was evaluated using a range of ARTS concentrations against a fixed ATP concentration. The affinity was calculated as 135 nM indicating that the bispecific design does not significantly alter TCR-CD3ε aptamer's affinity in the bispecific design (Figure 5F). We then tested the binding affinity of ARTS against Jurkat E6.1 cells using a fixed ARTS

https://doi.org/10.1021/acsomega.1c04125
ACS Omega 2021, 6, 32563−32570

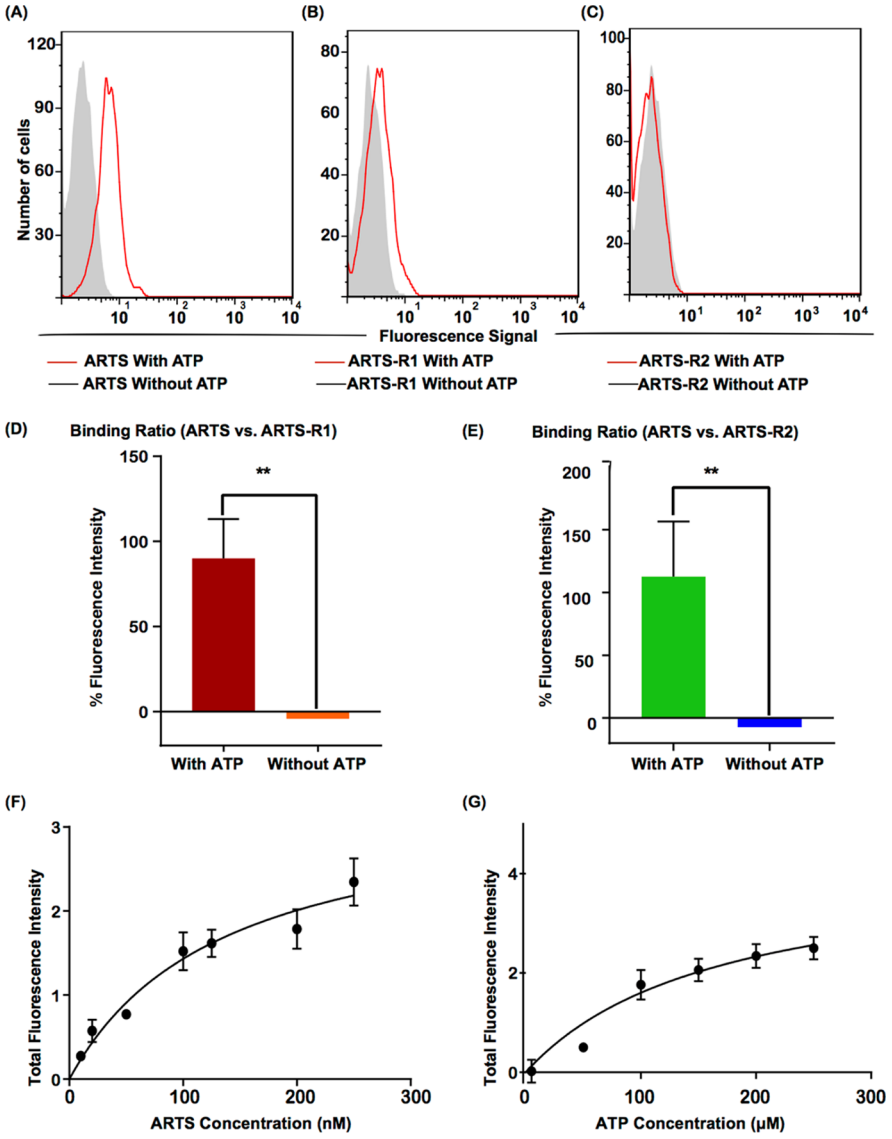

Figure 5. Analysis of specificity and affinity of ARTS, ARTS-R1, and ARTS-R2 against TCR-CD3ε expressed on Jurkat E6.1 cells. (A) Flow cytometry binding assay of ARTS targeting Jurkat E6.1 cells in the presence of ATP (red) and in the absence of ATP (gray). (B) Flow cytometry binding assay of ARTS-R1 targeting Jurkat E6.1 cells in the presence of ATP (red) and in the absence of ATP (gray). (C) Flow cytometry binding assay of ARTS-R2 in the presence of ATP (red) and in the absence of ATP (gray). All were folded by preincubating with either 500 μM ATP or without ATP, followed by incubation with 1×10^5 Jurkat E6.1 cells for 1 h in CSB. (D) Binding ratio of ARTS in the presence and absence of ATP using ARTS-R1's background fluorescence signal. (E) Binding ratio of ARTS in the presence and absence of ATP using ARTS-R2's fluorescence background. The results were analyzed using the one-way ANOVA with the Student's *t*-test performed on GraphPad Prism **: $p = 0.0021$, **: $p = 0.0009$. (F) Affinity curve of ARTS against Jurkat E6.1 cells as a function of ARTS concentration (10, 20, 50, 100, 125, 200, and 250 nM). (G) Affinity curve of ARTS against Jurkat E6.1 cells plotted as a function of ATP concentration (10, 100, 200, 300, 400, and 500 μM).

concentration of 100 nM with varying concentrations of ATP (Figure 5G) to evaluate whether the bispecific design had altered the affinity of the ATP aptamer toward ATP. We observed no significant change to the ATP aptamer's affinity to ATP (K_d = 334.2 μM), suggesting again, that the functional fold of the ATP binding aptamer segment in the bispecific design is uninterrupted. In normal tissues, the extracellular concentration of ATP is detected to be relatively low, ranging from 10 to 100 nM, whereas reports have shown that the extracellular concentration of ATP within the TME can reach over 100 μM.[13,14] Given that the affinity of the ATP aptamer toward the ATP is 334.2 mM, we used a concentration of 500 mM of ATP in cellular assays. Thus, the specificity of the anti-CD3ε aptamer in ARTS was further evaluated using TCR-CD3 negative cell lines (Figures S5 and S6). Also, we used ARTS and ARTS-R1 in the presence of 500 μM ATP with Jurkat E6.1 cells (Figure S5A), Ramos cells (Figure S5B), and CA46 cells (Figure S5C). The overall binding ratio between ARTS and ARTS-R1 using TCR-CD3 positive and negative cell lines (Figure S5D) shows that the ARTS specifically detects only TCR-CD3ε positive Jurkat E6.1 cells in response to the ATP concentration. The analysis of binding of ARTS and ARTS-R2 to Jurkat E6.1 cells in the absence and presence of 500 μM ATP (Figure S6A) using control Ramos cells (Figure S6B) and CA 46 cells (Figures S5C and S6D) confirms the specificity of ARTS toward Jurkat E6.1 cells mediated by the conformational switch induced by ATP. Collectively, the observed high specificity of ARTS against CD3ε-expressing

https://doi.org/10.1021/acsomega.1c04125
ACS Omega 2021, 6, 32563−32570

Jurkat E6.1 cells, suggests the specificity, robustness, and general applicability of this bispecific design in tumor detection.

CONCLUSIONS

DNA-based systems, specifically aptamers, serve as a promising molecular tool owing to their low cost and easily modifiable synthetic analogs with favorable pharmacokinetic properties to design modular DNA architectures.[26−29] Bispecific designs of aptamers has been evaluated for therapeutic development before.[30,31] However, to our knowledge, there are no bispecific aptamers, designs have been explored for sensing and detection. We herein demonstrated a DNA aptamer-based bispecific system to enhance the specificity of tumor cell detection by utilizing the unique biochemical composition of the TME. This dual-specific design exploited both the dynamic nature of DNA self-assembly and the specific recognition ability of aptamers toward small molecules and proteins. By combining these features, we introduced a *de novo*, *in situ* aptamer-based sensor as a superior platform for sensing tumor cells with added specificity to the biochemical features of the TME. We showed that the ARTS could be activated in the presence of a high concentration of ATP, and that T-cell binding was only promoted under these conditions. Thus, our prototype design introduces a novel concept of sensor design while expanding the aptamer versatility in the design of sensors and smart diagnostic platforms.

EXPERIMENTAL SECTION

Cell Cultures and Reagents. Jurkat, Clone E6.1 (T lymphocyte), cells were purchased from the American Type Culture Collection. The cell line was cultured in HyClone RPMI-1640 [+25 mM *N*-(2-hydroxyethyl)piperazine-*N*′-ethanesulfonic acid (HEPES) + L-glutamine] medium supplemented with 100 units/mL penicillin−streptomycin 1% (corning), 1% MEM non-essential amino acids (Gibco), and 10% fetal bovine serum (heat inactivated, Gibco). All cell lines were routinely evaluated on a flow cytometer (FACScan, Becton Dickinson) for the expression of CD marker using anti-hCD3ε (PE-conjugated Mouse IgG1, R&D Systems) antibody to authenticate the cell line. All conformational assays were tested using ATP, from a stock solution of 100 mM (Thermo Fisher). The specificity assay was performed using 2 mM of ATP, UTP, CTP, and GTP, from a stock solution of 100 mM (Thermo Fisher). All aptamer solutions were prepared in 10 mM tris-HCl (Thermo Scientific) adjusted to pH = 8.4, with 6 mM $MgCl_2$ (Sigma-Aldrich) from a stock solution of 1 M tris-HCl (Thermo Fisher). All DNA sequences were ordered high-performance liquid chromatography-purified from Integrated DNA Technologies and dual-modified with 6-carboxyfluorescein (6-FAM) and Iowa Black fluorescence quencher (IBFQ) at the 5′ and 3′, respectively.

Preparation of Solutions. All bispecific molecules, ARTS, ARTS-R1, and ARTS-R2, were reconstituted in 10 mM tris-HCl, pH = 8.4, to make a 100 μM stock solution, gently shaken for 3 h, and then refrigerated overnight to dissolve. Afterward, the accurate concentrations of each aptamer were determined using a UV−vis spectrophotometer (Thermo Scientific) at a 260 nm wavelength. A sub-stock solution of 10 μM was prepared for all aptamer molecules by the dilution of each of the respective stock solutions with 10 mM tris-HCl, pH = 8.4, and 6 mM $MgCl_2$ buffer to prepare the various working solutions.

Cell Binding Buffers. All binding assays were performed using a cell suspension buffer (CSB) composed of HyClone RPMI-1640 (+25 mM HEPES + L-glutamine) medium containing 200 mg/L tRNA (Sigma-Aldrich), 2 g/L bovine serum albumin (Fisher Scientific), and a 200 mg/L salmon sperm DNA solution (Invitrogen).

Aptamer Folding Conditions. Prior to mixing with cells for binding assays, the aptamers were prepared in 10 mM tris-HCl, pH = 8.4, and 6 mM $MgCl_2$ buffer placed in 95 °C for 5 min to denature undesired secondary structures, followed by cooling down to 25 °C in a 5% CO_2 incubator for 30 min to fold into the most stable secondary structure in the presence of ATP.

Thermal Stability of the Aptamer. To check thermal stability, 250 nM of each molecule (in 500 μL 10 mM, tris-HCl, pH = 8.4, and 6 mM $MgCl_2$) was placed in a Supermicro quartz cuvette for fluorescence measurements using the Cary Eclipse fluorescence spectrophotometer with a Cary temperature controller (Agilent). The emission wavelength used in the thermal stability assays was the emission wavelength of the 6-FAM fluorophore λ_{em} = 520 nm, and the excitation wavelength was λ_{ex} = 495 at different time points (each 5 min) with temperature changes from 10 to 90 °C.

Investigation of Aptamer Conformation. All molecules (ARTS, ART-R1, and ARTS-R2) were prepared in a final volume of 500 μL 10 mM tris-HCl, pH = 8.4, with 6 mM $MgCl_2$, to make a final concentration of 250 nM. All molecules were folded, as described above, transferred to a Supermicro quartz cuvette, and then placed in the Cary Eclipse fluorescence spectrophotometer at 25 °C. The fluorescence intensity of ARTS was measured at different concentrations of ATP in the range of 0−4 mM. The solutions were mixed well prior to fluorescence measurements. The excitation wavelength of the 6-FAM fluorophore was λ_{ex} = 495 nm, and the emission was scanned between λ_{em} = 505 and 600 nm. The emission slit was 5 nm, whereas the excitation slit was 10 nm. The fluorescence intensity of each molecule was measured in the absence of ATP and then in the presence of ATP at final concentrations of 0.5−4 mM. The mean of three separate measurements of 0−2 mM ATP concentrations was plotted to study the ATP-dependent fluorescence.

Specificity of ARTS toward ATP over GTP, UTP, and CTP. Prior to starting the specificity assay, 250 nM of each construct in 500 μL tris-HCl (10 mM, pH = 8.4, and 6 mM $MgCl_2$) was folded and mixed with 2 mM of each nucleotide (ATP, UTP, GTP, and CTP). The solutions were transferred to a quartz cuvette and placed in a fluorescence spectrophotometer at 25 °C. The excitation wavelength of the 6-FAM fluorophore was λ_{ex} = 495 nm, and the emission was scanned between λ_{em} = 505 and 600 nm. The emission slit was 5 nm, whereas the excitation slit was 10 nm.

Cell Binding Assays. Jurkat E6.1 cells were prepared by washing three times with 3 mL of HyClone RPMI-1640 (+25 mM HEPES + L-glutamine) medium prior to aptamer binding. All sequences were prepared at an initial concentration of 200 nM from 1 μM sub-stock solutions in 10 mM tris-HCl, pH = 8.4, and 6 mM $MgCl_2$. Prior to mixing aptamers with the cells, 200 nM of ATRS or control molecules in tris-HCl (10 mM, pH = 8.4, and 6 mM $MgCl_2$) were folded at 95 °C for 5 min and then transferred to 25 °C for 30 min.

https://doi.org/10.1021/acsomega.1c04125
ACS Omega 2021, 6, 32563−32570

After folding, 75 μL of ARTS with and without ATP were mixed with 75 μL of 1×10^5 Jurkat E 6.1 in the CSB to give a final concentration of 100 nM for the aptamer molecule and 500 μM for ATP in a total volume of 150 μL. A equal volume of buffer was added to the sample that served as a control without ATP. Binding of each aptamer was analyzed using flow cytometry by counting 5000 events. As a positive control, Jurkat E6.1 cell lines were incubated with 5 μL of 25 μg/mL anti-hCD3ε antibody (PE-conjugated Mouse IgG1, R&D Systems) or 2 μL of 200 μg/mL isotype control (PE Mouse IgG1, κ, BD Biosciences) for 30 min on ice, followed by washing with 2 mL of RPMI-1640 medium and reconstitution in 250 μL of RPMI-1640 medium. Binding events were monitored in FL1 green (515−545 nm) for the aptamer and in FL2 yellow (565−605; 564−606 nm) for the antibody, counting 5000 events using flow cytometry.

Specificity Assay with Different Cell Lines. Jurkat E6.1, Ramos, and CA46 cells were prepared by washing three times with 3 mL HyClone RPMI-1640 (+25 mM HEPES + L-glutamine) medium prior to aptamer binding to the cells. All sequences were prepared at an initial concentration of 200 nM from 1 μM sub-stock solutions in 10 mM tris-HCl, pH = 8.4, and 6 mM $MgCl_2$. Aptamers and cells were first mixed; then 200 nM of each construct in tris-HCl (10 mM, pH = 8.4, and 6 mM $MgCl_2$) was folded at 95 °C for 5 min and then transferred to 25 °C for 30 min.

After folding, 75 μL of each construct sample were mixed with 75 μL containing 1×10^5 of each cell line in the CSB to give a final concentration of 100 nM for the ARTS constructs and 500 μM for ATP (5 μL from a stock solution of 100 mM) in a total volume of 150 μL. An equal volume of the buffer was added to the sample that served as a control without ATP. Binding of each aptamer was analyzed using flow cytometry by counting 5000 events. As a positive control, Jurkat E6.1 cells were incubated with 5 μL of 25 μg/mL anti-hCD3ε antibody (PE-conjugated Mouse IgG1, R&D Systems) or 2 μL of 200 μg/mL isotype control (PE Mouse IgG1, κ, BD Biosciences) for 30 min on ice, followed by a one-time wash with 2 mL of RPMI-1640 medium and reconstitution in 250 μL of RPMI-1640 medium. As a negative control, Ramos and CA46 cell lines were incubated with 5 μL of 25 μg/mL anti-hCD3ε antibody (PE-conjugated Mouse IgG1, R&D Systems) or 2 μL of 200 μg/mL isotype control (PE Mouse IgG1, κ, BD Biosciences) for 30 minutes on ice, followed by a one-time wash with 2 mL of RPMI-1640 medium and reconstitution in 250 μL of RPMI-1640 medium. Binding events were monitored in FL1 green (515−545 nm) for the aptamer and in FL2 yellow (565−605; 564−606 nm) for the antibody, counting 5000 events using flow cytometry.

■ ASSOCIATED CONTENT

Supporting Information

The Supporting Information is available free of charge at https://pubs.acs.org/doi/10.1021/acsomega.1c04125.

Experimental results for titration assays of control molecules, ATRS-R1, ARTS-R2 with ATP and specificity assays for control molecules, ATRS-R1, ARTS-R2 against cell lines (PDF)

■ AUTHOR INFORMATION

Corresponding Author

Prabodhika Mallikaratchy − *Department of Chemistry, Lehman College, The City University of New York, Bronx, New York 10468, United States; Ph.D. Programs in Chemistry and Biochemistry and Ph.D. Program in Molecular, Cellular and Developmental Biology, CUNY Graduate Center, New York, New York 10016, United States;* orcid.org/0000-0002-6437-4613; Phone: 347-577-4082; Email: prabodhika.mallikaratchy@lehman.cuny.edu

Authors

Natalie Boykoff − *Ph.D. Programs in Chemistry and Biochemistry, CUNY Graduate Center, New York, New York 10016, United States*

Lina Freage − *Department of Chemistry, Lehman College, The City University of New York, Bronx, New York 10468, United States*

Jared Lenn − *The Bronx High School of Science, Bronx, New York 10468, United States*

Complete contact information is available at: https://pubs.acs.org/10.1021/acsomega.1c04125

Author Contributions

⊥N.B. and L.F. equally contributed.

Notes

The authors declare no competing financial interest.

■ ACKNOWLEDGMENTS

The authors are grateful for funding for this work by the National Institute of General Medical Sciences Grant SC1 GM122648 and R35 GM139336-01.

■ REFERENCES

(1) Reina-Campos, M.; Moscat, J.; Diaz-Meco, M. Metabolism shapes the tumor microenvironment. *Curr. Opin. Cell Biol.* **2017**, *48*, 47−53.

(2) Hsu, P. P.; Sabatini, D. M. Cancer cell metabolism: Warburg and beyond. *Cell* **2008**, *134*, 703−707.

(3) Palm, W.; Thompson, C. B. Nutrient acquisition strategies of mammalian cells. *Nature* **2017**, *546*, 234−242.

(4) Quail, D. F.; Joyce, J. A. Microenvironmental regulation of tumor progression and metastasis. *Nat. Med.* **2013**, *19*, 1423−1437.

(5) Pavlova, N. N.; Thompson, C. B. The Emerging Hallmarks of Cancer Metabolism. *Cell Metab.* **2016**, *23*, 27−47.

(6) Joyce, J. A.; Fearon, D. T. T cell exclusion, immune privilege, and the tumor microenvironment. *Science* **2015**, *348*, 74−80.

(7) Vijayan, D.; Young, A.; Teng, M. W. L.; Smyth, M. J. Targeting immunosuppressive adenosine in cancer. *Nat. Rev. Cancer* **2017**, *17*, 765.

(8) Hu, Q.; Huang, Z.; Duan, Y.; Fu, Z.; Bin Liu, L. Reprogramming Tumor Microenvironment with Photothermal Therapy. *Bioconjugate Chem.* **2020**, *31*, 1268−1278.

(9) Dong, Y.; Dong, S.; Wang, Z.; Feng, L.; Sun, Q.; Chen, G.; He, F.; Liu, S.; Li, W.; Yang, P. Multimode Imaging-Guided Photothermal/Chemodynamic Synergistic Therapy Nanoagent with a Tumor Microenvironment Responded Effect. *ACS Appl. Mater. Interfaces* **2020**, *12*, 52479−52491.

(10) Gillies, R. J.; Raghunand, N.; Karczmar, G. S.; Bhujwalla, Z. M. MRI of the tumor microenvironment. *J Magn. Reson. Imag.* **2002**, *16*, 430−450.

(11) Joyce, J. A.; Pollard, J. W. Microenvironmental regulation of metastasis. *Nat. Rev. Cancer* **2009**, *9*, 239−252.

(12) Scharping, N. E.; Delgoffe, G. M. Tumor Microenvironment Metabolism: A New Checkpoint for Anti-Tumor Immunity. *Vaccines* **2016**, *4*, 46.
(13) Gilbert, S. M.; Oliphant, C. J.; Hassan, S.; Peille, A. L.; Bronsert, P.; Falzoni, S.; Di Virgilio, F.; McNulty, S.; Lara, R. ATP in the tumour microenvironment drives expression of nfP2X7, a key mediator of cancer cell survival. *Oncogene* **2019**, *38*, 194−208.
(14) Allard, B.; Longhi, M. S.; Robson, S. C.; Stagg, J. The ectonucleotidases CD39 and CD73: Novel checkpoint inhibitor targets. *Immunol. Rev.* **2017**, *276*, 121−144.
(15) Di Virgilio, F.; Sarti, A. C.; Falzoni, S.; De Marchi, E.; Adinolfi, E. Extracellular ATP and P2 purinergic signalling in the tumour microenvironment. *Nat. Rev. Cancer* **2018**, *18*, 601−618.
(16) Koudrina, A.; DeRosa, M. C. Advances in Medical Imaging: Aptamer- and Peptide-Targeted MRI and CT Contrast Agents. *ACS Omega* **2020**, *5*, 22691−22701.
(17) Kufer, P.; Lutterbüse, R.; Baeuerle, P. A. A revival of bispecific antibodies. *Trends Biotechnol.* **2004**, *22*, 238−244.
(18) Byrne, H.; Conroy, P. J.; Whisstock, J. C.; O'Kennedy, R. J. A tale of two specificities: bispecific antibodies for therapeutic and diagnostic applications. *Trends Biotechnol.* **2013**, *31*, 621−632.
(19) Hernandez-Lopez, R. A.; Yu, W.; Cabral, K. A.; Creasey, O. A.; Lopez Pazmino, M. D. P.; Tonai, Y.; De Guzman, A.; Mäkelä, A.; Saksela, K.; Gartner, Z. J.; Lim, W. A. T cell circuits that sense antigen density with an ultrasensitive threshold. *Science* **2021**, *371*, 1166−1171.
(20) Cui, F.; Yue, Y.; Zhang, Y.; Zhang, Z.; Zhou, H. S. Advancing Biosensors with Machine Learning. *ACS Sens.* **2020**, *5*, 3346−3364.
(21) Lim, C. Z. J.; Zhang, L.; Zhang, Y.; Sundah, N. R.; Shao, H. New Sensors for Extracellular Vesicles: Insights on Constituent and Associated Biomarkers. *ACS Sens.* **2020**, *5*, 4−12.
(22) Di, Z.; Zhao, J.; Chu, H.; Xue, W.; Zhao, Y.; Li, L. An Acidic-Microenvironment-Driven DNA Nanomachine Enables Specific ATP Imaging in the Extracellular Milieu of Tumor. *Adv. Mater.* **2019**, *31*, No. e1901885.
(23) Huizenga, D. E.; Szostak, J. W. A DNA aptamer that binds adenosine and ATP. *Biochemistry* **1995**, *34*, 656−665.
(24) Zumrut, H. E.; Batool, S.; Argyropoulos, K. V.; Williams, N.; Azad, R.; Mallikaratchy, P. R. Integrating Ligand-Receptor Interactions and In Vitro Evolution for Streamlined Discovery of Artificial Nucleic Acid Ligands. *Mol. Ther. Nucleic Acids* **2019**, *17*, 150−163.
(25) Kim, Y.; Yang, C. J.; Tan, W. Superior structure stability and selectivity of hairpin nucleic acid probes with an L-DNA stem. *Nucleic Acids Res.* **2007**, *35*, 7279−7287.
(26) Freage, L.; Boykoff, N.; Mallikaratchy, P. Utility of Multivalent Aptamers to Develop Nanoscale DNA Devices against Surface Receptors. *ACS Omega* **2021**, *6*, 12382−12391.
(27) Freage, L.; Jamal, D.; Williams, N. B.; Mallikaratchy, P. R. A Homodimeric Aptamer Variant Generated from Ligand-Guided Selection Activates the T Cell Receptor Cluster of Differentiation 3 Complex. *Mol. Ther. Nucleic Acids* **2020**, *22*, 167−178.
(28) Keller, A.; Linko, V. Challenges and Perspectives of DNA Nanostructures in Biomedicine. *Angew. Chem., Int. Ed. Engl.* **2020**, *59*, 15818−15833.
(29) Nummelin, S.; Shen, B.; Piskunen, P.; Liu, Q.; Kostiainen, M. A.; Linko, V. Robotic DNA Nanostructures. *ACS Synth. Biol.* **2020**, *9*, 1923−1940.
(30) Tang, Z.; Mallikaratchy, P.; Yang, R.; Kim, Y.; Zhu, Z.; Wang, H.; Tan, W. Aptamer switch probe based on intramolecular displacement. *J. Am. Chem. Soc.* **2008**, *130*, 11268−11269.
(31) Boltz, A.; Piater, B.; Toleikis, L.; Guenther, R.; Kolmar, H.; Hock, B. Bi-specific aptamers mediating tumor cell lysis. *J. Biol. Chem.* **2011**, *286*, 21896−21905.

https://doi.org/10.1021/acsomega.1c04125
ACS Omega 2021, 6, 32563−32570